

RADIALLY SYMMETRIC SOLUTIONS OF THE ULTRA-RELATIVISTIC EULER EQUATIONS

MATTHIAS KUNIK, HAILIANG LIU, AND GERALD WARNECKE

Dedicated to Professor Hsiao Ling on the occasion of her 80th birthday

ABSTRACT. The ultra-relativistic Euler equations for an ideal gas are described in terms of the pressure p , the spatial part $\underline{u} \in \mathbb{R}^3$ of the dimensionless four-velocity and the particle density n . Radially symmetric solutions of these equations are studied. Analytical solutions are presented for the linearized system. For the original nonlinear equations we design and analyze a numerical scheme for simulating radially symmetric solutions in three space dimensions. The good performance of the scheme is demonstrated by numerical examples. In particular, it was observed that the method has the capability to capture accurately the pressure singularity formation caused by shock wave reflections at the origin.

1. INTRODUCTION

Relativistic flow problems are vital in many astrophysical phenomena. An effective way to improve our knowledge of the actual mechanisms is due to relativistic hydrodynamics simulations. Especially, solutions describing radially symmetric gas flow are important in applications as well as in theory. They are particularly well suited for numerical simulations of certain multi-dimensional problems. In this paper we focus on radially symmetric solutions. We consider a special relativistic system which is much simpler than flows in general relativistic theory. Interestingly, even compared to the classical Euler equations of non-relativistic gas dynamics the equations we consider exhibit a simpler mathematical structure.

We are concerned with the ultra-relativistic equations for a perfect fluid in Minkowski space-time, namely

$$(1.1) \quad \sum_{\beta=0}^3 \frac{\partial T_{\alpha\beta}}{\partial x_\beta} = 0, \quad \frac{\partial N_\alpha}{\partial x_\alpha} = 0,$$

where

$$T_{\alpha\beta} = -pg_{\alpha\beta} + 4pu_\alpha u_\beta$$

Date: February 5, 2020.

2010 Mathematics Subject Classification. 35L45, 35L60, 35L65, 35L67.

Key words and phrases. Relativistic Euler equations, conservation laws, hyperbolic systems, Lorentz transformations, shock waves, entropy conditions, rarefaction waves.

denotes the energy-momentum tensor for the ideal ultra-relativistic gas. Here p represents the pressure, $\underline{u} \in \mathbb{R}^3$ is the spatial part of the four-velocity $(u_0, u_1, u_2, u_3) = (\sqrt{1 + |\underline{u}|^2}, \underline{u})$. The flat Minkowski metric is given as

$$g_{\alpha\beta} = \begin{cases} +1, & \alpha = \beta = 0, \\ -1, & \alpha = \beta = 1, 2, 3, \\ 0, & \alpha \neq \beta, \end{cases}$$

and the particle-density four-vector is denoted by

$$(1.2) \quad N_\alpha = nu_\alpha.$$

Here n is the proper particle density. We note that the quantities u_α , $T_{\alpha\beta}$, $g_{\alpha\beta}$, N_α and even x_α are usually written down as Lorentz-invariant tensors with *upper indices* instead of lower indices in order to make use of Einstein's summation convention. But in the following calculations these upper indices could be mixed up with powers. Since we will not make use of the lowering and raising of Lorentz-tensor indices, our change of the notation will not lead to confusions. For the physical background we refer to Weinberg [22, Part one, pp 47-52], further details can be found in Kunik [10, Chapter 3.9], and for the corresponding classical Euler equations see Courant and Friedrichs [5]. For a general introduction to the mathematical theory of hyperbolic conservation laws see Bressan [4] and Dafermos [6]. A nice overview of radially symmetric solutions to conservation laws is given in Jenssen's survey paper [9].

The unknown quantities p , \underline{u} and n satisfying (1.1) depend in general on time $t = x_0 \geq 0$ and position $\underline{x} = (x_1, x_2, x_3) \in \mathbb{R}^3$. It is well known that even for smooth initial data, where the fields are prescribed at $t = 0$, the solution may develop shock discontinuities. This requires a weak form of the conservation laws in (1.1). Since the conservation law for the particle-density four-vector (1.2) decouples from the conservation laws of energy and momentum, we will restrict ourselves to the resulting closed subsystem for the variables p and \underline{u} satisfying the first set of equations in (1.1). Putting $\alpha = 0$ this gives the conservation of energy

$$(1.3) \quad \frac{\partial}{\partial t} (3p + 4p|\underline{u}|^2) + \sum_{k=1}^3 \frac{\partial}{\partial x_k} (4pu_k \sqrt{1 + |\underline{u}|^2}) = 0,$$

whereas for $\alpha = j = 1, 2, 3$ we obtain the conservation of momentum

$$(1.4) \quad \frac{\partial}{\partial t} (4pu_j \sqrt{1 + |\underline{u}|^2}) + \sum_{k=1}^3 \frac{\partial}{\partial x_k} (p\delta_{jk} + 4pu_j u_k) = 0, \quad j = 1, 2, 3.$$

Like the classical Euler equations, these relativistic Euler equations constitute a hyperbolic system of conservation laws and have their origin in the

kinetic theory of gases. This can be used for the construction of numerical schemes which preserve positive pressure and satisfy a discrete version of the entropy inequality, see [10, 11, 13]. Some other analytical and numerical methods for the ultra relativistic Euler equations are studied in [1, 2, 3, 8, 12, 15, 16, 17, 18]. Recently numerical results using central upwind scheme are reported in [7] for one and two dimensional special ultra-relativistic Euler equations. In [14] Lai presents a detailed analysis of self-similar solutions of radially symmetric relativistic Euler equations in three and two space dimensions. These are special solutions depending only on r/t with radius r and time t which satisfy systems of ordinary differential equations. Especially his study of the ultra-relativistic Euler equations enables us to compare his solutions with two of our numerical results.

In this paper, we study radially symmetric solutions and construct a corresponding scheme to solve the ultra-relativistic Euler equations (1.3), (1.4) in three space dimensions. One of the main advantages of the radially symmetric problem is that it can be used to efficiently simulate special wave patterns for fully three dimensional problems such as the detonation problem, see [21]; also Example 5.5 in [20] for the classical Euler equations. We show this with Example 4 in Section 5 for the ultra-relativistic Euler equations. This allows the prediction of pressure singularity formation caused by shock wave reflections at the origin. The shock wave reflection with a pressure singularity at the boundary is also motivated by the analysis of the linearized model in Section 3. We hope that our specific solutions may become benchmarks for testing fully 3D simulations.

In the next section we will define radially symmetric solutions of (1.3), (1.4) in a weak integral form. We will also present the initial- and boundary value problem for nonlinear radially symmetric solutions. In Section 3 we will especially solve the corresponding linearized model, which reveals singularities in the pressure field due to shock reflections at the boundary. Formulation and analysis of a stable scheme based on the balance laws (2.13) are presented in Section 4. In this connection emphasis is on a proper treatment of the radius and the boundary conditions in the balance laws. The numerical examples are given in Section 5.

2. RADIALLY SYMMETRIC SOLUTIONS

Assume for a moment a smooth solution p, \underline{u} of the ultra-relativistic Euler equations (1.3), (1.4). We put $r = |\underline{x}|$ for $r \geq 0$ and look for radially

symmetric solutions

$$(2.1) \quad p = p(t, r) > 0, \quad \underline{u}(t, \underline{x}) = \frac{u(t, r)}{r} \underline{x}.$$

Here the quantity $\underline{u}(t, \underline{x}) \in \mathbb{R}^3$ is completely determined by a new *real valued quantity* $u(t, r)$ depending on $t > 0$, $r > 0$. For continuity we have the boundary condition

$$(2.2) \quad \lim_{r \downarrow 0} u(t, r) = 0, \quad t > 0.$$

Note that $\underline{n} = \frac{1}{r} \underline{x}$ is the outer normal vector field of the sphere $\partial \mathcal{B}_R$ bounding the ball $\mathcal{B}_R = \{\underline{x} \in \mathbb{R}^3 : |\underline{x}| \leq R\}$ of radius $R > 0$, and that $|\underline{u}|^2 = u^2$ as well as $u = \underline{u} \cdot \underline{n}$. Therefore, it is natural to apply the Gaussian divergence theorem for the integration of the second term with respect to \mathcal{B}_R of the conservation law (1.3) in order to make use of the radial symmetry of the fields. We obtain with (2.1) for any fixed $R > 0$

$$4\pi \frac{\partial}{\partial t} \int_0^R (3p(t, r) + 4p(t, r)u^2(t, r)) r^2 dr + \int_{\partial \mathcal{B}_R} 4pu\sqrt{1+u^2} dS = 0.$$

The integrand in the surface integral is constant. Hence we have

$$(2.3) \quad \begin{aligned} & \frac{\partial}{\partial t} \int_0^R (3p(t, r) + 4p(t, r)u^2(t, r)) r^2 dr \\ & + R^2 4p(t, R)u(t, R)\sqrt{1+u^2(t, R)} = 0. \end{aligned}$$

This idea does not work for the momentum equation (1.4), because (2.1) would give values zero after integration with respect to \mathcal{B}_R . Here we integrate (1.4) for $j = 3$ over the upper half-ball

$$\mathcal{B}_R^+ = \{\underline{x} = (x_1, x_2, x_3) \in \mathbb{R}^3 : x_3 \geq 0\},$$

use the Gaussian divergence theorem and spherical coordinates

$$x_1 = r \cos \varphi \sin \vartheta, \quad x_2 = r \sin \varphi \sin \vartheta, \quad x_3 = r \cos \vartheta$$

with $r > 0$, $0 < \varphi < 2\pi$ and $0 < \vartheta < \pi/2$, and obtain from (2.1)

$$(2.4) \quad \begin{aligned} & \frac{\partial}{\partial t} \int_0^R 4p(t, r)u(t, r)\sqrt{1+u^2(t, r)} r^2 dr \\ & + R^2 (4p(t, R)u^2(t, R) + p(t, R)) = 2 \int_0^R p(t, r) r dr. \end{aligned}$$

Now we differentiate the equations (2.3), (2.4) with respect to $R > 0$. Afterwards we replace R by the better suited variable $x > 0$.

We put $p = p(t, x)$, $u = u(t, x)$ for abbreviation and have the 2 by 2 system

$$(2.5) \quad \begin{cases} \frac{\partial}{\partial t} (x^2 p(3 + 4u^2)) + \frac{\partial}{\partial x} (4x^2 p u \sqrt{1 + u^2}) = 0, \\ \frac{\partial}{\partial t} (4x^2 p u \sqrt{1 + u^2}) + \frac{\partial}{\partial x} (x^2 p(1 + 4u^2)) = 2xp. \end{cases}$$

The validity of this system may also be checked by differentiation from (2.1), (1.3) and (1.4). The solutions of (2.5) are restricted to the state space $\mathcal{S}_{eul} = \{(p, u) \in \mathbb{R}^2 : p > 0\}$.

For the formulation of weak entropy solutions we will introduce a transformation in state space. With $\tilde{\mathcal{S}}_{eul} = \{(a, b) \in \mathbb{R}^2 : |b| < a\}$ there is a one-to-one transformation $\Theta : \mathcal{S}_{eul} \mapsto \tilde{\mathcal{S}}_{eul}$ given by

$$(2.6) \quad \Theta(p, u) = \begin{pmatrix} p(3 + 4u^2) \\ 4pu\sqrt{1 + u^2} \end{pmatrix} = \begin{pmatrix} a \\ b \end{pmatrix}.$$

The inverse transformation is given by

$$p = \frac{1}{3} \left(\sqrt{4a^2 - 3b^2} - a \right), \quad u = \frac{b}{\sqrt{4p(p + a)}}.$$

Using the transformation (2.6) in state space we can also rewrite (2.5) in an equivalent form. We put

$$(2.7) \quad c = c(a, b) = \frac{5}{3}a - \frac{2}{3}\sqrt{4a^2 - 3b^2},$$

and obtain from (2.5), (2.6)

$$(2.8) \quad \begin{cases} \frac{\partial}{\partial t} (x^2 a) + \frac{\partial}{\partial x} (x^2 b) = 0, \\ \frac{\partial}{\partial t} (x^2 b) + \frac{\partial}{\partial x} (x^2 c) = x(a - c). \end{cases}$$

We look for weak solutions of (2.8) in the quarterplane

$$Q = \{(t, x) : t > 0, x > 0\}.$$

For $x > 0$ we prescribe the *two initial functions*

$$(2.9) \quad \lim_{t \downarrow 0} a(t, x) = a_0(x), \quad \lim_{t \downarrow 0} b(t, x) = b_0(x), \quad x > 0$$

with $|b_0(x)| < a_0(x)$ for $x > 0$. Recall our preliminary assumption that we have a smooth and radially symmetric solution of the three dimensional ultra-relativistic Euler equations (1.3) and (1.4), which implies the boundary condition (2.2) as well as a locally bounded energy and momentum density. Hence we have the following *two boundary conditions* for $t > 0$:

$$(2.10) \quad \lim_{x \downarrow 0} (x^2 a(t, x)) = 0, \quad \lim_{x \downarrow 0} b(t, x) = 0.$$

We recall (2.7), multiply in both equations of (2.8) with any C^1 test function $\phi : \mathbb{R}^2 \mapsto \mathbb{R}$ with compact support in \mathbb{R}^2 and obtain from (2.10) after partial integration

$$(2.11) \quad \left\{ \begin{array}{l} \iint_Q \left(a \frac{\partial \phi}{\partial t} + b \frac{\partial \phi}{\partial x} \right) x^2 dx dt + \int_0^\infty a_0 \phi_0 x^2 dx = 0, \\ \iint_Q \left(b \frac{\partial \phi}{\partial t} + c(a, b) \frac{\partial \phi}{\partial x} \right) x^2 dx dt \\ + \iint_Q (a - c(a, b)) \phi x dx dt + \int_0^\infty b_0 \phi_0 x^2 dx = 0. \end{array} \right.$$

We use $\phi = \phi(t, x)$, $\frac{\partial \phi}{\partial t} = \frac{\partial \phi}{\partial t}(t, x)$, $\frac{\partial \phi}{\partial x} = \frac{\partial \phi}{\partial x}(t, x)$, $a = a(t, x)$, $b = b(t, x)$, $\phi_0 = \phi(0, x)$, $a_0 = a_0(x)$, $b_0 = b_0(x)$ as abbreviations in (2.11). Now we drop the assumption that we have a smooth solution of the ultra-relativistic Euler equations and will no longer assume that a and b are locally bounded.

Definition 2.1. Weak radially symmetric solutions

We say that a, b is a *weak solution* of (2.8) with initial data a_0, b_0 if and only if the following conditions are satisfied:

- $a, b : Q \mapsto \mathbb{R}$ are measurable with $|b| < a$.
- $xa(t, x)$ is integrable in $(0, t_0) \times (0, x_0) \subset Q$ for all $t_0, x_0 > 0$.
- $a_0, b_0 : \mathbb{R}_{>0} \mapsto \mathbb{R}$ are measurable with $|b_0| < a_0$. We require for all $x_0 > 0$ that $xa_0(x)$ is integrable for $0 < x < x_0$.
- The boundary conditions (2.10) are satisfied for almost all $t > 0$.
- Equations (2.11) are satisfied for all C^1 test function $\phi : \mathbb{R}^2 \mapsto \mathbb{R}$ with compact support in \mathbb{R}^2 .

If $\psi : Q \mapsto \mathbb{R}_{\geq 0}$ is a new *nonnegative* C^1 test function restricted to the quarter plane Q with compact support in Q , then we will consider a weak solution a, b which further satisfies the *weak entropy inequality*, see Kunik [10, Chapter 4.4],

$$(2.12) \quad \iint_Q \left(p^{3/4} \sqrt{1+u^2} \frac{\partial \psi}{\partial t} + p^{3/4} u \frac{\partial \psi}{\partial x} \right) x^2 dx dt \leq 0.$$

Here we make use of $\Theta(p, u) = \begin{pmatrix} a \\ b \end{pmatrix}$ in (2.6). In this case we call a, b a *weak entropy solution* of the system (2.8). \square

Remark 2.2. Properties of weak entropy solutions

- 1) It follows from the assumptions in Definition 2.1 for a, b, a_0 and b_0 that all the integrals in (2.11) and (2.12) are well defined. For (2.11)

we first note that xa is locally integrable. From $|b| < a$ and (2.7) we conclude that xb and $xc(a, b)$ are locally integrable as well. For the entropy inequality we make use of (2.6) and obtain

$$p^{3/4}\sqrt{1+u^2} = 2^{-7/4}(3a - c(a, b))^{1/2}(a - c(a, b))^{1/4}.$$

With $\frac{a}{3} \leq c(a, b) < a$ we have $p^{3/4}|u| \leq p^{3/4}\sqrt{1+u^2} \leq (a/3)^{3/4}$ and conclude that the integral in (2.12) is well defined.

- 2) At all points of smoothness any solution p, u satisfying (2.5) will also satisfy the entropy conservation law

$$\frac{\partial}{\partial t} \left(x^2 p^{3/4} \sqrt{1+u^2} \right) + \frac{\partial}{\partial x} \left(x^2 p^{3/4} u \right) = 0.$$

In this case the additional conservation law can be obtained from (2.5) by a straightforward but lengthy calculation.

- 3) In the presence of shock waves (2.12) will satisfy the strict inequality in general, and we obtain a simple evaluation of (2.12), see [1, Chapter 2.1] for more details: If for $p_-, p_+ > 0$ the left state (p_-, u_-) can be connected to the right state (p_+, u_+) by a single shock satisfying the Rankine-Hugoniot jump conditions, then this shock wave satisfies the entropy inequality if and only if $u_- > u_+$. This condition can also be checked easily for the numerical solutions with shock curves in Chapter 5.

In [10] we have used contour integrals for weak solutions of conservation laws, following Oleinik's formulation [19] for a scalar conservation law. Here we recall the definition (2.7) of c , make use of the abbreviations $a = a(t, x)$, $b = b(t, x)$ and obtain an alternative formulation of (2.11) if we require especially for a piecewise smooth weak solution a, b and for each convex domain $\Omega \subset Q$ with piecewise smooth boundary $\partial\Omega \subset Q$:

$$(2.13) \quad \begin{aligned} \int_{\partial\Omega} x^2 a \, dx - x^2 b \, dt &= 0, \\ \int_{\partial\Omega} x^2 b \, dx - x^2 c \, dt &= \iint_{\Omega} x(a - c) \, dt dx. \end{aligned}$$

3. SOLUTIONS OF THE LINEARIZED SYSTEM

A linearized version of the system (2.8) is given by

$$(3.1) \quad \begin{cases} \frac{\partial}{\partial t} (x^2 a) + \frac{\partial}{\partial x} (x^2 b) = 0, \\ \frac{\partial}{\partial t} (x^2 b) + \frac{\partial}{\partial x} \left(\frac{x^2}{3} a \right) = \frac{2x}{3} a. \end{cases}$$

We linearize at the state $(a, b) = (a, 0)$. The system can be obtained by neglecting the terms b^2 in (2.8). For $t = 0$ and $x \geq 0$ we prescribe initial data $a_0(x) = a(0, x)$, $b_0(x) = b(0, x)$ and assume that $b_0(0) = 0$. From the radial symmetry the variable $x > 0$ corresponds to the radius variable. Now we want to extend our initial data to all of \mathbb{R} using symmetry in order to obtain simple solution formulas. For $x > 0$ we extend a_0 to an *even function* with $a_0(-x) = a_0(x)$ and b_0 to an *odd function* with $b_0(-x) = -b_0(x)$. Now we assume that $a_0, b_0 : \mathbb{R} \mapsto \mathbb{R}$ are both C^1 -functions. For $x \in \mathbb{R}$ we define the two *even primitive functions*

$$(3.2) \quad A_0(x) = \int_0^x u a_0(u) du, \quad B_0(x) = \int_0^x b_0(u) du.$$

Theorem 3.1. *The solution of (3.1) satisfying the initial conditions*

$$\lim_{t \downarrow 0} a(t, x) = a_0(x), \quad \lim_{t \downarrow 0} b(t, x) = b_0(x), \quad x > 0,$$

is given for all $t > 0$, $x > 0$ by

$$(3.3) \quad \begin{aligned} a(t, x) = & \frac{1}{2x} \left(x + \frac{t}{\sqrt{3}} \right) a_0 \left(x + \frac{t}{\sqrt{3}} \right) \\ & + \frac{1}{2x} \left(x - \frac{t}{\sqrt{3}} \right) a_0 \left(x - \frac{t}{\sqrt{3}} \right) \\ & - \frac{\sqrt{3}}{2x} \left[\left(x + \frac{t}{\sqrt{3}} \right) b_0 \left(x + \frac{t}{\sqrt{3}} \right) + B_0 \left(x + \frac{t}{\sqrt{3}} \right) \right] \\ & + \frac{\sqrt{3}}{2x} \left[\left(x - \frac{t}{\sqrt{3}} \right) b_0 \left(x - \frac{t}{\sqrt{3}} \right) + B_0 \left(x - \frac{t}{\sqrt{3}} \right) \right], \end{aligned}$$

$$(3.4) \quad \begin{aligned} b(t, x) = & -\frac{1}{2\sqrt{3}x} \left[\left(x + \frac{t}{\sqrt{3}} \right) a_0 \left(x + \frac{t}{\sqrt{3}} \right) - \frac{1}{x} A_0 \left(x + \frac{t}{\sqrt{3}} \right) \right] \\ & + \frac{1}{2\sqrt{3}x} \left[\left(x - \frac{t}{\sqrt{3}} \right) a_0 \left(x - \frac{t}{\sqrt{3}} \right) - \frac{1}{x} A_0 \left(x - \frac{t}{\sqrt{3}} \right) \right] \\ & + \frac{1}{2x} \left[\left(x + \frac{t}{\sqrt{3}} \right) b_0 \left(x + \frac{t}{\sqrt{3}} \right) - \frac{1}{x} \cdot \frac{t}{\sqrt{3}} B_0 \left(x + \frac{t}{\sqrt{3}} \right) \right] \\ & + \frac{1}{2x} \left[\left(x - \frac{t}{\sqrt{3}} \right) b_0 \left(x - \frac{t}{\sqrt{3}} \right) + \frac{1}{x} \cdot \frac{t}{\sqrt{3}} B_0 \left(x - \frac{t}{\sqrt{3}} \right) \right]. \end{aligned}$$

Proof. Assume that $F'_0 = f_0$ for any C^2 -function F_0 . If we make the ansatz

$$(3.5) \quad \begin{aligned} a_+(t, x) &= \frac{1}{x} f_0 \left(x + \frac{t}{\sqrt{3}} \right), \\ b_+(t, x) &= -\frac{1}{\sqrt{3}x} f_0 \left(x + \frac{t}{\sqrt{3}} \right) + \frac{1}{\sqrt{3}x^2} F_0 \left(x + \frac{t}{\sqrt{3}} \right), \end{aligned}$$

then we can easily check that $a_+, b_+ : Q \mapsto \mathbb{R}$ satisfy (3.1) with

$$\lim_{t \downarrow 0} a_+(t, x) = \frac{f_0(x)}{x}, \quad \lim_{t \downarrow 0} b_+(t, x) = -\frac{f_0(x)}{\sqrt{3}x} + \frac{F_0(x)}{\sqrt{3}x^2}, \quad x > 0.$$

In the same way

$$(3.6) \quad \begin{aligned} a_-(t, x) &= \frac{1}{x} f_0 \left(x - \frac{t}{\sqrt{3}} \right), \\ b_-(t, x) &= \frac{1}{\sqrt{3}x} f_0 \left(x - \frac{t}{\sqrt{3}} \right) - \frac{1}{\sqrt{3}x^2} F_0 \left(x - \frac{t}{\sqrt{3}} \right), \end{aligned}$$

also satisfy (3.1) for $t > 0, x > 0$ with

$$\lim_{t \downarrow 0} a_-(t, x) = \frac{f_0(x)}{x}, \quad \lim_{t \downarrow 0} b_-(t, x) = \frac{f_0(x)}{\sqrt{3}x} - \frac{F_0(x)}{\sqrt{3}x^2}, \quad x > 0.$$

Using (3.2), (3.5) and (3.6) we can check that (3.3) and (3.4) satisfy (3.1) line by line in the following way:

For the first line on the right-hand side in (3.3) and (3.4) we put $F_0(x) = \frac{1}{2} A_0(x)$ and use (3.5), for the second line we put again $F_0(x) = \frac{1}{2} A_0(x)$ and use (3.6), and the third and fourth line with $F_0(x) = -\frac{\sqrt{3}}{2} x B_0(x)$, (3.5) and $F_0(x) = +\frac{\sqrt{3}}{2} x B_0(x)$, (3.6), respectively. In this way the initial conditions are also obtained. \square

Remark 3.2. It follows from the previous theorem that $x a(t, x)$ and $x b(t, x)$ are even bounded in any bounded subdomain of the quarterplane $t, x > 0$.

However, for more general weak solutions $|a(t, x)|$ and $|b(t, x)|$ may become infinitely large in certain small time intervals for $x \downarrow 0$. This is shown in the following example with a spherical imploding shock: We first use (3.2). Put $b_0(x) = B_0(x) = 0$ for all $x \in \mathbb{R}$ and

$$a_0(x) = \begin{cases} 1 & \text{for } |x| < 1, \\ 2 & \text{for } |x| \geq 1. \end{cases}$$

Then we have the even function

$$A_0(x) = \int_0^x u a_0(u) du = \begin{cases} \frac{1}{2} x^2 & \text{for } |x| < 1, \\ x^2 - \frac{1}{2} & \text{for } |x| \geq 1. \end{cases}$$

We define, as seen in Figure 1, the convex domains

$$\begin{aligned} \Omega_1 &= \{ (t, x) \in \mathbb{R}_{>0} \times \mathbb{R}_{>0} : x \leq 1 - t/\sqrt{3} \}, \\ \Omega_2 &= \{ (t, x) \in \mathbb{R}_{>0} \times \mathbb{R}_{>0} : |1 - t/\sqrt{3}| < x \leq 1 + t/\sqrt{3} \}, \\ \Omega_3 &= \{ (t, x) \in \mathbb{R}_{>0} \times \mathbb{R}_{>0} : x > 1 + t/\sqrt{3} \}, \\ \Omega_4 &= \{ (t, x) \in \mathbb{R}_{>0} \times \mathbb{R}_{>0} : x \leq t/\sqrt{3} - 1 \} \end{aligned}$$

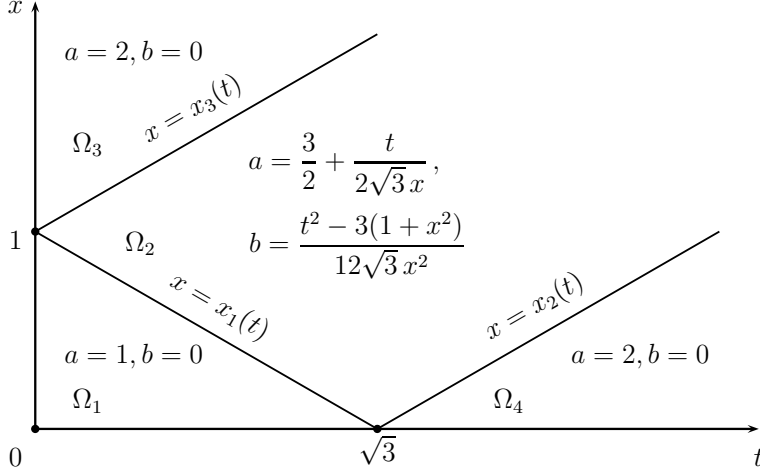


FIGURE 1. Solution of the linearized system.

and obtain from (3.3), (3.4):

$$a(t, x) = \begin{cases} 1 & \text{for } (t, x) \in \Omega_1, \\ \frac{3}{2} + \frac{t}{2\sqrt{3}x} & \text{for } (t, x) \in \Omega_2, \\ 2 & \text{for } (t, x) \in \Omega_3 \cup \Omega_4, \end{cases}$$

$$b(t, x) = \begin{cases} 0 & \text{for } (t, x) \in \Omega_1 \cup \Omega_3 \cup \Omega_4, \\ \frac{t^2 - 3(1+x^2)}{12\sqrt{3}x^2} & \text{for } (t, x) \in \Omega_2. \end{cases}$$

We can easily check that a, b satisfy the differential equations (3.1) in the interior of each Ω_j , $j = 1, 2, 3, 4$. Moreover, for $i = 1, 2, 3$ the Rankine-Hugoniot jump conditions

$$\dot{x}_i(t) = \lim_{\varepsilon \downarrow 0} \frac{b(t, x_i(t) + \varepsilon) - b(t, x_i(t) - \varepsilon)}{a(t, x_i(t) + \varepsilon) - a(t, x_i(t) - \varepsilon)} = \pm \frac{1}{\sqrt{3}}$$

of the linearized system are satisfied across the three shocks

$$\begin{aligned} x_1(t) &= 1 - \frac{t}{\sqrt{3}}, & 0 < t < \sqrt{3}, \\ x_2(t) &= \frac{t}{\sqrt{3}} - 1, & t > \sqrt{3}, \\ x_3(t) &= 1 + \frac{t}{\sqrt{3}}, & t > 0, \end{aligned}$$

see Figure 1. Theorem 3.1 gives a weak solution of the linearized system even if the initial functions a_0, b_0 have jump discontinuities.

Theorem 3.3. *Take the assumptions as in Theorem 3.1. If b_0, a_0 are both C^2 -functions, then we have $\lim_{x \downarrow 0} b(t, x) = 0$ for all $t > 0$.*

Proof. L'Hospital's rule can be applied twice to obtain the desired radial limit. \square

The linearized system serves as a motivation for the following study of the nonlinear system. However, we cannot expect a quantitatively similar behaviour between both models concerning the shock-wave reflection and the singular structure near the boundary, where nonlinear momentum terms cannot be neglected.

4. FORMULATION OF A STABLE NUMERICAL SCHEME

We develop a stable numerical scheme for the initial value problem with the radially symmetric ultra-relativistic Euler equations. The method of contour-integration for the formulation of the balance laws (2.13) is used to construct a function called "Euler" which enables the evolution in time of the numerical solution on a staggered grid, i.e. it allows us to construct the solution (a', b') at the next time step from the solution (a_{\pm}, b_{\pm}) in two neighboring gridpoints at the former time step according to Figure 3. First we determine the computational domain and define some quantities which are needed for its discretization.

- 1) Given are $t_*, x_* > 0$ in order to calculate a numerical solution of the initial value problem (2.13), (2.9) in the time range $[0, t_*]$ and the spatial range $[0, x_*]$.
- 2) We want to use a staggered grid scheme. Any given number $N \in \mathbb{N}$ with $N \cdot x_* \geq t_*$ determines the time step size

$$\Delta t = \frac{t_*}{2N}.$$

The time steps are

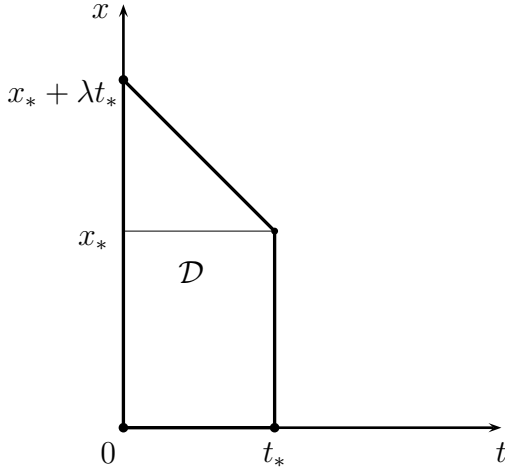
$$t_n = (n - 1)\Delta t, \quad n = 1, \dots, 2N + 1.$$

- 3) Put

$$M = \left\lfloor \frac{x_*}{t_*} N \right\rfloor \geq 1,$$

then the spatial mesh size is

$$\Delta x = \frac{x_*}{M},$$

FIGURE 2. The computational domain \mathcal{D}

with the spatial grid points

$$x_j = (j - 1)\Delta x, \quad j = 1, \dots, N + M + 1.$$

Note that our scheme uses a trapezoidal computational domain \mathcal{D} defined below that includes the target domain $[0, t_*] \times [0, x_*]$. Thereby, we can use all initial data that influence the solution on the target domain. In this way we avoid using a numerical boundary condition at x_* .

4) The number

$$\lambda = \frac{\Delta x}{2\Delta t} \geq 1$$

is used to satisfy the CFL-condition and to define the computational domain $\mathcal{D} = \{(t, x) \in \mathbb{R}^2 : 0 \leq t \leq t_*, \quad 0 \leq x \leq x_* + \lambda(t_* - t)\}$.

The typical trapezoidal form of the computational domain is illustrated in Figure 2.

For the formulation and the stability of our numerical scheme we need two lemmas.

Lemma 4.1. *Assume that $|b_{\pm}| < a_{\pm}$. We recall that $\lambda \geq 1$, (2.7) and put $c_{\pm} = c(a_{\pm}, b_{\pm})$. Then*

$$\begin{aligned} \text{a)} \quad & - \left(a_- + \frac{b_-}{\lambda} \right) < b_- + \frac{c_-}{\lambda} < a_- + \frac{b_-}{\lambda}, \\ \text{b)} \quad & - \left(a_+ - \frac{b_+}{\lambda} \right) < b_+ - \frac{c_+}{\lambda} < a_+ - \frac{b_+}{\lambda}. \end{aligned}$$

Proof. The proof of b) is quite analogous to a), hence we will only show a). The left inequality in a) is equivalent with $\lambda(a_- + b_-) > -c_- - b_-$, and due to $\lambda \geq 1$ and $a_- + b_- > 0$ it is sufficient to show $a_- + b_- > -c_- - b_-$. We

have

$$\begin{aligned}
 & a_- + b_- > -c_- - b_- \\
 \Leftrightarrow & 2a_- + \frac{3}{2}b_- > \sqrt{a_-^2 - \frac{3}{4}b_-^2} \quad \text{with } 2a_- + \frac{3}{2}b_- > 0 \\
 \Leftrightarrow & 4a_-^2 + 6a_-b_- + \frac{9}{4}b_-^2 > a_-^2 - \frac{3}{4}b_-^2 \\
 \Leftrightarrow & 3(a_- + b_-)^2 > 0,
 \end{aligned}$$

which shows the left inequality. The right inequality in a) is equivalent to $\lambda(a_- - b_-) > c_- - b_-$. Due to $\lambda \geq 1$ and $a_- - b_- > 0$ it is sufficient to show $a_- > c_-$. We have

$$\begin{aligned}
 & a_- > c_- \\
 \Leftrightarrow & 2\sqrt{a_-^2 - \frac{3}{4}b_-^2} > a_- \quad \text{with } a_- > 0 \\
 \Leftrightarrow & 4a_-^2 - 3b_-^2 > a_-^2 \\
 \Leftrightarrow & 3(a_-^2 - b_-^2) > 0.
 \end{aligned}$$

□

Lemma 4.2. *Assume that $a > 0$, $0 < \eta \leq 1/3$ and $-a(1+\eta) < \xi < a(1-\eta)$. Then we obtain $4a^2(1+3\eta^2) - 3\xi^2 > 0$ and*

$$\left| \frac{\xi + \eta\sqrt{4a^2(1+3\eta^2) - 3\xi^2}}{1+3\eta^2} \right| < a.$$

Proof. We have

$$4a^2(1+3\eta^2) - 3\xi^2 > 4a^2(1+3\eta^2) - 3a^2(1+\eta)^2 = a^2(1-3\eta)^2 \geq 0,$$

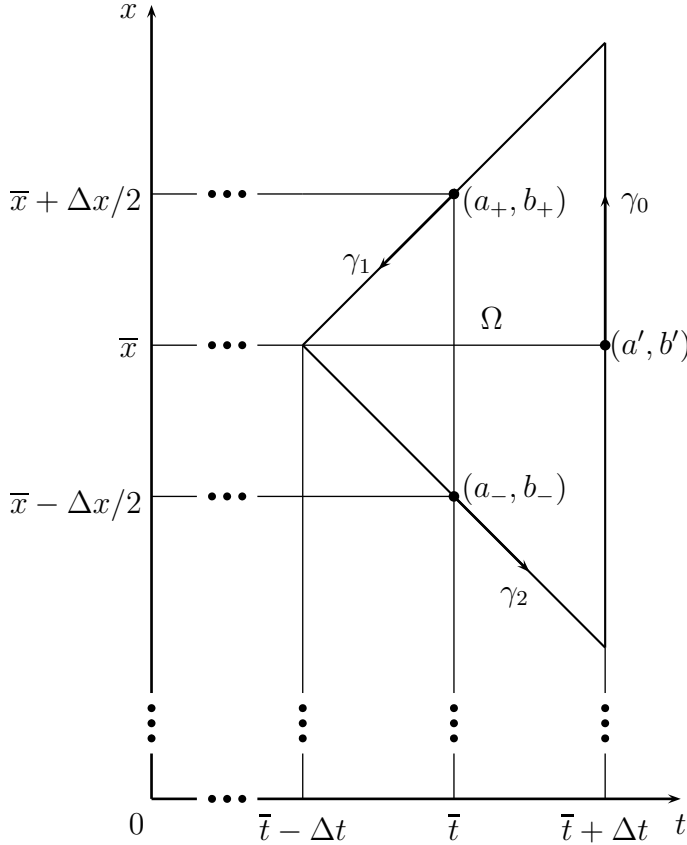
and the square root in the estimate of the lemma is well defined. To show the estimate we use $0 < \eta \leq 1/3$ and first note that

$$\begin{aligned}
 & \frac{-a(1+\eta) + \eta\sqrt{4a^2(1+3\eta^2) - 3(-a(1+\eta))^2}}{1+3\eta^2} = -a, \\
 & \frac{a(1-\eta) + \eta\sqrt{4a^2(1+3\eta^2) - 3(a(1-\eta))^2}}{1+3\eta^2} = a.
 \end{aligned}$$

Therefore it is sufficient for the proof of the lemma to show that

$$B(\xi) = \xi + \eta\sqrt{4a^2(1+3\eta^2) - 3\xi^2}$$

is strictly monotonically increasing for $-a(1+\eta) < \xi < a(1-\eta)$. The condition $B'(\xi) = 0$ gives $3\eta\xi = \sqrt{4a^2(1+3\eta^2) - 3\xi^2}$, hence $\xi > 0$ and the

FIGURE 3. The balance region Ω

unique solution $\xi = \frac{2a}{\sqrt{3}} > a(1 - \eta)$ outside the interval. On the other hand we have $B'(0) = 1 > 0$. Hence B is strictly increasing in the interval. \square

For the numerical discretization of the system (2.13) we choose the triangular balance domain Ω depicted in Figure 3. We assume that the midpoints $P_- = (\bar{t}, \bar{x} - \Delta x/2)$, $P_+ = (\bar{t}, \bar{x} + \Delta x/2)$ and $P' = (\bar{t} + \Delta t, \bar{x})$ of the cords of $\partial\Omega$ are numerical gridpoints for the computational domain \mathcal{D} . Let the numerical solution (a_{\pm}, b_{\pm}) be given at the gridpoints P_{\pm} . We have to require $|b_{\pm}| < a_{\pm}$ for the numerical solution in the actual time step $\bar{t} = t_n$ with $t = 1, \dots, 2N$. The major task is to calculate the numerical solution (a', b') for the next time step $\bar{t} + \Delta t = t_{n+1}$ at its gridpoint P' , see Figure 3.

The spatial value $\bar{x} \geq 0$ is given. We have to determine a function

$$(4.1) \quad \text{Euler}(a_-, b_-, a_+, b_+, \bar{x}, \Delta x, \lambda) = (a', b')$$

for the calculation of (a', b') . This leads to the structure of a staggered grid scheme. Note that at the boundary the balance region Ω may have parts outside \mathcal{D} , e.g. points below the half-space $x \geq 0$. In the latter case we will

employ a simple reflection principle for the numerical solution in order to use the function Euler as well for the evaluation of the boundary conditions.

Next we will make use of the fact that the points P_{\pm} with numerical values (a_{\pm}, b_{\pm}) and P' with unknown value (a', b') are the *midpoints of the three boundary cords* of the balance region Ω . We put $c_{\pm} = c(a_{\pm}, b_{\pm})$ and $c' = c(a', b')$ for abbreviation, see (2.7). Then we use for $k = 0, 1, 2$ the straight line paths γ_k from Figure 3 and for the corresponding path integrals

$$\int_{\gamma_k} x^2 a(t, x) dx - x^2 b(t, x) dt \quad \text{and} \quad \int_{\gamma_k} x^2 b(t, x) dx - x^2 c(a(t, x), b(t, x)) dt$$

with the unknown weak entropy solution $a(t, x)$, $b(t, x)$ their numerical discretizations $I_{k,a}$ and $I_{k,b}$, respectively, given by

(4.2)

$$\begin{aligned} I_{0,a} &= \int_{\gamma_0} x^2 a' dx - x^2 b' dt = a' \int_{\bar{x}-\Delta x}^{\bar{x}+\Delta x} x^2 dx = 4a'\lambda\Delta t \left(\bar{x}^2 + \frac{1}{3}(\Delta x)^2 \right), \\ I_{0,b} &= \int_{\gamma_0} x^2 b' dx - x^2 c' dt = b' \int_{\bar{x}-\Delta x}^{\bar{x}+\Delta x} x^2 dx = 4b'\lambda\Delta t \left(\bar{x}^2 + \frac{1}{3}(\Delta x)^2 \right). \end{aligned}$$

(4.3)

$$\begin{aligned} I_{1,a} &= \int_{\gamma_1} x^2 a_+ dx - x^2 b_+ dt = -2(\lambda a_+ - b_+)\Delta t \left(\bar{x}^2 + \frac{1}{3}(\Delta x)^2 + \bar{x}\Delta x \right), \\ I_{1,b} &= \int_{\gamma_1} x^2 b_+ dx - x^2 c_+ dt = -2(\lambda b_+ - c_+)\Delta t \left(\bar{x}^2 + \frac{1}{3}(\Delta x)^2 + \bar{x}\Delta x \right). \end{aligned}$$

(4.4)

$$\begin{aligned} I_{2,a} &= \int_{\gamma_2} x^2 a_- dx - x^2 b_- dt = -2(\lambda a_- + b_-)\Delta t \left(\bar{x}^2 + \frac{1}{3}(\Delta x)^2 - \bar{x}\Delta x \right), \\ I_{2,b} &= \int_{\gamma_2} x^2 b_- dx - x^2 c_- dt = -2(\lambda b_- + c_-)\Delta t \left(\bar{x}^2 + \frac{1}{3}(\Delta x)^2 - \bar{x}\Delta x \right). \end{aligned}$$

We recall that $\bar{x} \geq 0$ and put

$$(4.5) \quad q = \frac{2\bar{x}\Delta x}{\bar{x}^2 + \frac{1}{3}(\Delta x)^2} < 2.$$

The numerical discretization of the first balance law in (2.13) gives

$$(4.6) \quad I_{0,a} = -I_{1,a} - I_{2,a}.$$

We obtain from (4.2), (4.3), (4.4), (4.5) and (4.6) for a' the explicit solution

$$(4.7) \quad a' = \frac{1}{2} \left(a_- + \frac{b_-}{\lambda} \right) (1 - q/2) + \frac{1}{2} \left(a_+ - \frac{b_+}{\lambda} \right) (1 + q/2).$$

For the numerical discretization of the second balance law in (2.13) we approximate the integral

$$\iint_{\Omega} x(a - c) dt dx$$

by

$$(a' - c') \iint_{\Omega} x dt dx = 2(a' - c') \bar{x} \Delta t \Delta x.$$

Now (4.2), (4.3), (4.4) give the following ansatz for the calculation of b' :

$$(4.8) \quad I_{0,b} = -I_{1,b} - I_{2,b} + 2(a' - c') \bar{x} \Delta t \Delta x.$$

Recall $c_{\pm} = c(a_{\pm}, b_{\pm})$ with $c = c(a, b)$ in (2.7). We use the abbreviations

$$(4.9) \quad \xi = \frac{1}{2} \left(b_- + \frac{c_-}{\lambda} \right) (1 - q/2) + \frac{1}{2} \left(b_+ - \frac{c_+}{\lambda} \right) (1 + q/2) - \frac{a' q}{6\lambda}, \quad \eta = \frac{q}{6\lambda}.$$

From (4.8) we obtain the implicit equation

$$(4.10) \quad b' = \xi + \eta \sqrt{4a'^2 - 3b'^2}.$$

This leads to a quadratic equation for b' . Lemma 4.1 gives

$$-a'(1 + \eta) < \xi < a'(1 - \eta)$$

for the quantity a' in (4.7). In order to apply Lemma 4.2 with a' instead of a we have to choose the solution

$$(4.11) \quad b' = \frac{\xi + \eta \sqrt{4a'^2(1 + 3\eta^2) - 3\xi^2}}{1 + 3\eta^2}$$

of (4.10) with the positive square root. Now b' is well defined with $|b'| < a'$, see the transformation (2.6) in state space. We summarize our results in the following

Theorem 4.3. Numerical solution (a', b') for the balance region Ω

Given are real quantities $\bar{x} \geq 0$ and a_{\pm}, b_{\pm} . Assume that $|b_{\pm}| < a_{\pm}$. We recall $\lambda \geq 1$ defined in terms of Δt and Δx and put $c_{\pm} = c(a_{\pm}, b_{\pm})$ in the definition (2.7). Then we have $|b'| < a'$ for the quantities a' and b' calculated from (4.5), (4.7), (4.9) and (4.11). \square

Definition 4.4. The function Euler

The state (a', b') from Theorem 4.3 defines the function Euler in (4.1). \square

Remark 4.5. Assume that the state (a_+, b_+) with $|b_+| < a_+$ is given and that $\bar{x} = 0$. We define the "reflected state" $\mathcal{R}(a_+, b_+) = (a_+, -b_+)$ and obtain

$$(4.12) \quad \text{Euler}(a_+, -b_+, a_+, b_+, 0, \Delta x, \lambda) = (a_+ - b_+/\lambda, 0).$$

This means that numerical values (a', b') calculated with the function Euler in (4.1) at the boundary $\bar{x} = 0$ with reflected states $(a_-, b_-) = \mathcal{R}(a_+, b_+)$ satisfy the boundary condition $b' = 0$.

Now we are able to formulate the numerical scheme for the solution of the initial-boundary value problem (2.9), (2.10), (2.13). We construct staggered grid points in the computational domain \mathcal{D} and compute the numerical solution at these gridpoints. The function Euler enables the evolution of the numerical solution in time, i.e. it allows us to construct the solution at time $t = t_{n+1}$ from the solution which is already calculated in the gridpoints at the former time step $t = t_n$. Note that the triangular balance domains that we used to determine the routine Euler overlap. But this presents no problem since they are not needed once the formulas for new values have been obtained.

- The staggered gridpoints are $(t_n, x_{n,j}) \in \mathcal{D}$ for $t_n = (n - 1)\Delta t$, $n = 1, \dots, 2N + 1$ and $j = 1, \dots, M + N - \lfloor (n - 1)/2 \rfloor$ with

$$x_{n,j} = \begin{cases} (x_j + x_{j+1})/2 & \text{if } n \text{ is odd} \\ x_j & \text{if } n \text{ is even.} \end{cases}$$

We want to calculate the numerical solution $(a_{n,j}, b_{n,j})$ at $(t_n, x_{n,j})$.

- For $j = 1, \dots, M + N$ we calculate the numerical solution $(a_{1,j}, b_{1,j})$ at the gridpoint $(t_1, x_{1,j}) = (0, (x_j + x_{j+1})/2)$ from the given initial data by

$$a_{1,j} = a_0(x_{1,j}), \quad b_{1,j} = b_0(x_{1,j}).$$

This corresponds to taking the integral average of the initial data on (x_j, x_{j+1}) and using the midpoint rule as quadrature.

- Assume that for a fixed *odd index* $n \in \{1, \dots, 2N\}$ we have already determined the numerical solution $(a_{n,j}, b_{n,j})$ at the gridpoints $(t_n, x_{n,j})$, $j = 1, \dots, M + N - (n - 1)/2$.

First we determine the solution $(a_{n+1,1}, b_{n+1,1})$ at the boundary point $(t_{n+1}, x_{n+1,1}) = (t_{n+1}, 0)$ according to (4.12) in Remark 4.5. For this purpose we put $a_+ = a_{n,1}$, $b_+ = b_{n,1}$, $a_- = a_{n,1}$, $b_- = -b_{n,1}$ and have

$$(a_{n+1,1}, b_{n+1,1}) = \text{Euler}(a_-, b_-, a_+, b_+, 0, \Delta x, \lambda) \text{ with } b_{n+1,1} = 0.$$

Next we put $a_- = a_{n,j-1}$, $b_- = b_{n,j-1}$ and $a_+ = a_{n,j}$, $b_+ = b_{n,j}$ for $j = 2, \dots, M + N - (n - 1)/2$ and determine the values $a_{n+1,j}$, $b_{n+1,j}$ at time t_{n+1} and position $\bar{x} = x_{n+1,j} = x_j$ from

$$(a_{n+1,j}, b_{n+1,j}) = \text{Euler}(a_-, b_-, a_+, b_+, \bar{x}, \Delta x, \lambda).$$

- Assume that for a fixed *even index* $n \in \{1, \dots, 2N\}$ we have already determined the numerical solution $(a_{n,j}, b_{n,j})$ at the gridpoints $(t_n, x_{n,j})$, $j = 1, \dots, M + N - n/2 + 1$.

We put $a_- = a_{n,j}$, $b_- = b_{n,j}$ and $a_+ = a_{n,j+1}$, $b_+ = b_{n,j+1}$ for $j = 1, \dots, M + N - n/2$ and determine the values $a_{n+1,j}$, $b_{n+1,j}$ at time t_{n+1} and position $\bar{x} = x_{n+1,j} = (x_j + x_{j+1})/2$ from

$$(a_{n+1,j}, b_{n+1,j}) = \text{Euler}(a_-, b_-, a_+, b_+, \bar{x}, \Delta x, \lambda).$$

Based on Lemma 4.1 and 4.2 we obtained Theorem 4.3. This implies stability for our scheme, namely the following

Theorem 4.6. *The numerical scheme described above is stable, especially the numerical values for the pressure p always remain positive.* \square

5. NUMERICAL EXAMPLES

We solve the initial value problem (2.8), (2.9) numerically for different choices of the initial data a_0, b_0 . We make use of the transformation (2.6). However, for our numerical results we take the usual velocity

$$v = \frac{u}{\sqrt{1+u^2}} \quad \text{with } |v| < 1$$

instead of the four velocity u and the initial velocity $v_0 = v(0, \cdot)$. The restriction $|v| < 1$ leads to better color plots.

- 1) If $a_0 > 0$ is constant and $b_0 = 0$, then we obtain a stationary solution, which is exactly reconstructed with these values by the scheme in Section 4. This corresponds to $u = v = 0$ and constant pressure p . Such a steady part is contained in the following examples.
- 2) We choose the constant initial data $a_0 = 7$, $b_0 = 4\sqrt{2}$ corresponding to a constant initial pressure $p_0 = 1$ and a constant radial part $u_0 = 1$ and $v_0 = 1/\sqrt{2}$ of the initial four velocity and usual velocity, respectively.

The numerical approximation leads us to the assumption that the exact solution depends only on x/t . Indeed, the existence of such a self-similar solution is justified in Lai's recent paper [14, Theorem 1.1]. Then we have a region emanating from the zero point with a low constant pressure $p = 0.00032$ and zero velocity $v = 0$ for $t > 0$, followed by a centered rarefaction fan starting from the zero point above the region with the constant values. The numerical solution with $x_* = 1$, $t_* = 1$ and $N = 3000$ is given in the Figures 4 and 5.

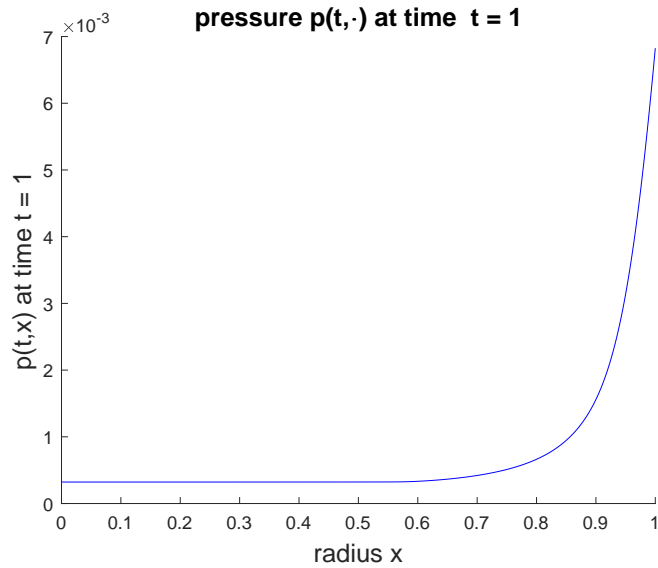


FIGURE 4. Pressure p at $t = 1$ from the second example

We also found that the computational values are in good agreement with those predicted from the results in Lai [14].

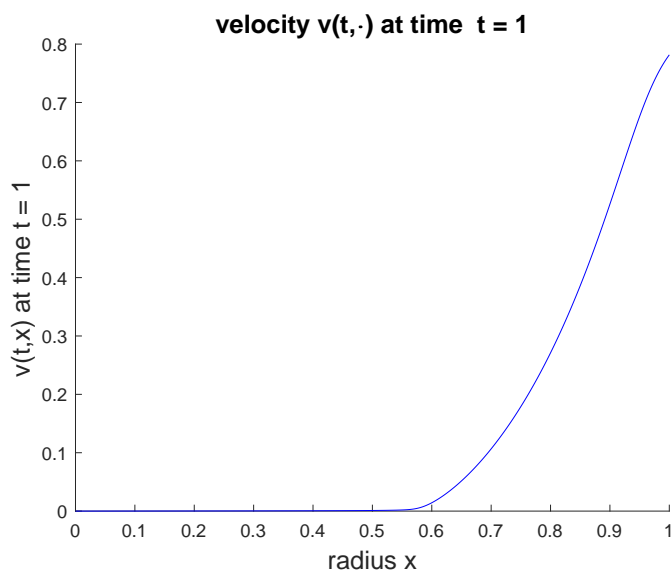


FIGURE 5. Velocity v at $t = 1$ from the second example

- 3) We choose the constant initial data $a_0 = 7$, $b_0 = -4\sqrt{2}$ corresponding to a constant initial pressure $p_0 = 1$ and a constant radial part $u_0 = -1$ and $v_0 = -1/\sqrt{2}$ of the initial four velocity and usual velocity, respectively. The exact solution again depends only on x/t ,

see [14, Theorem 1.1]. Here we observe a straight line shock wave with slope $s = 0.523$ emanating from the zero point, with a constant pressure $p = 25.55$ and zero velocity $v = 0$ for $t > 0$ below the shock wave, followed by a centered rarefaction fan starting from the zero point above the shock wave. The numerical solution with $x_* = 1$, $t_* = 1$ and $N = 3000$ is given in Figures 6 and 7.

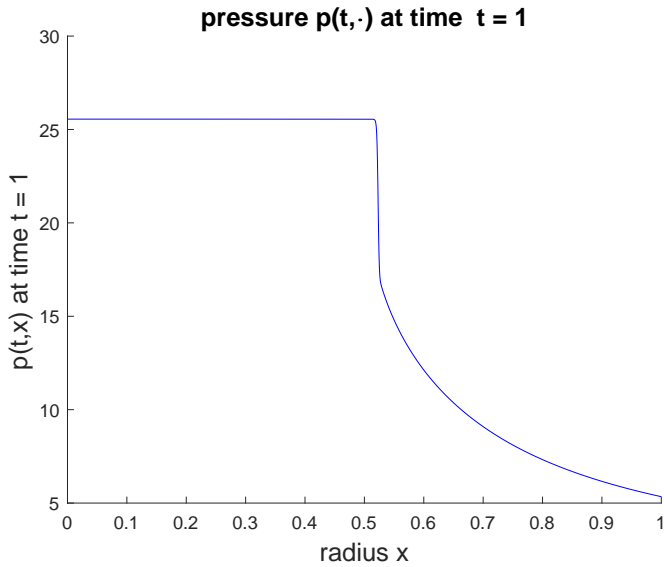


FIGURE 6. Pressure p at $t = 1$ from the third example

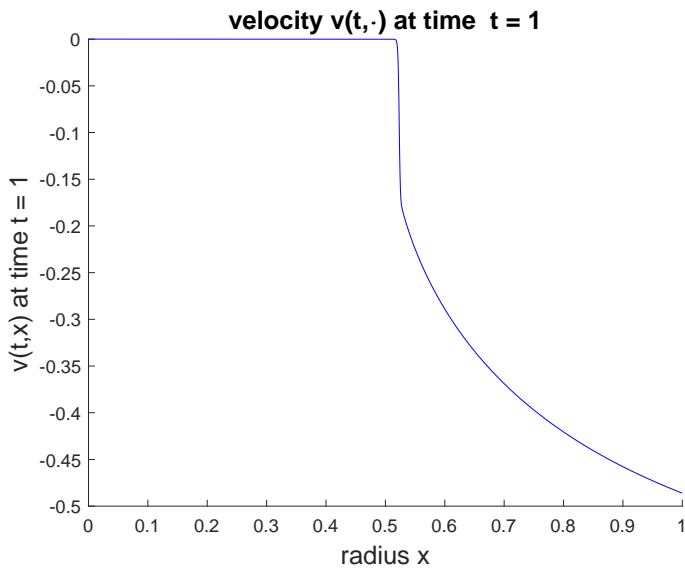


FIGURE 7. Velocity v at $t = 1$ from the third example

4) Expansion of a three dimensional spherical bubble with initial data

$$p_0(x) = \begin{cases} 1 & \text{for } 0 \leq x \leq 1 \\ 0.1 & \text{for } x > 1, \end{cases} \quad v_0(x) = 0.$$

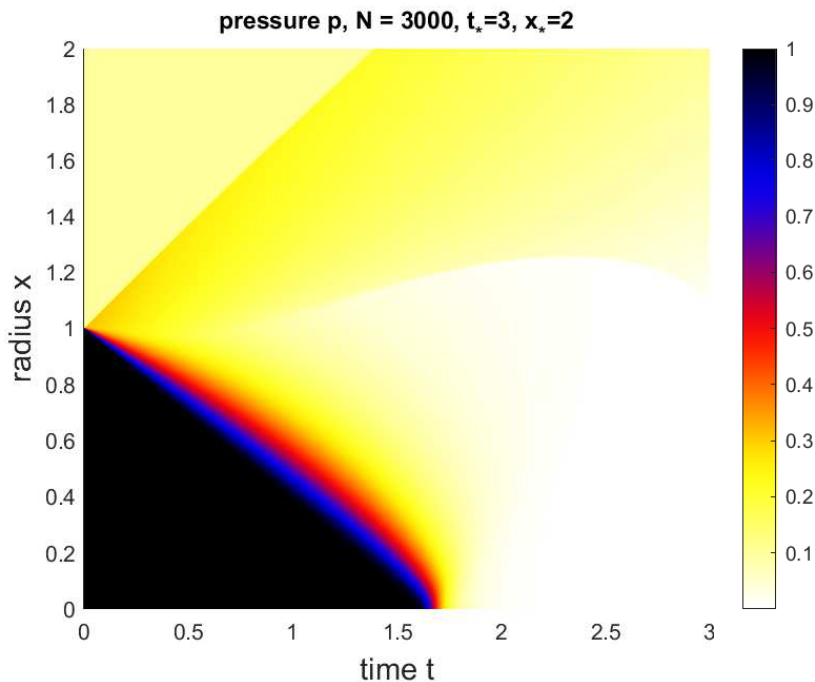


FIGURE 8. Pressure p from Example 4.

Initially, the pressure inside the bubble is ten times larger than outside, which leads to a fast expansion of the bubble into the outer low pressure area. This in turn gives rise to the formation of another low pressure area, namely the light yellow or white region in Figure 8 emanating from the zero point. The corresponding velocity is depicted in Figure 9. We observe the formation of a shock wave, running downwards into the new low pressure area and reaching the zero point around time $t = 4.16$, see Figures 10 and 11. The formation of this new shock wave is a peculiar nonlinear phenomenon. Shortly before the shock reaches the zero point the pressure takes very low values, but its reflection from the zero point causes a strong increase of the pressure in a very small time-space range near the boundary.

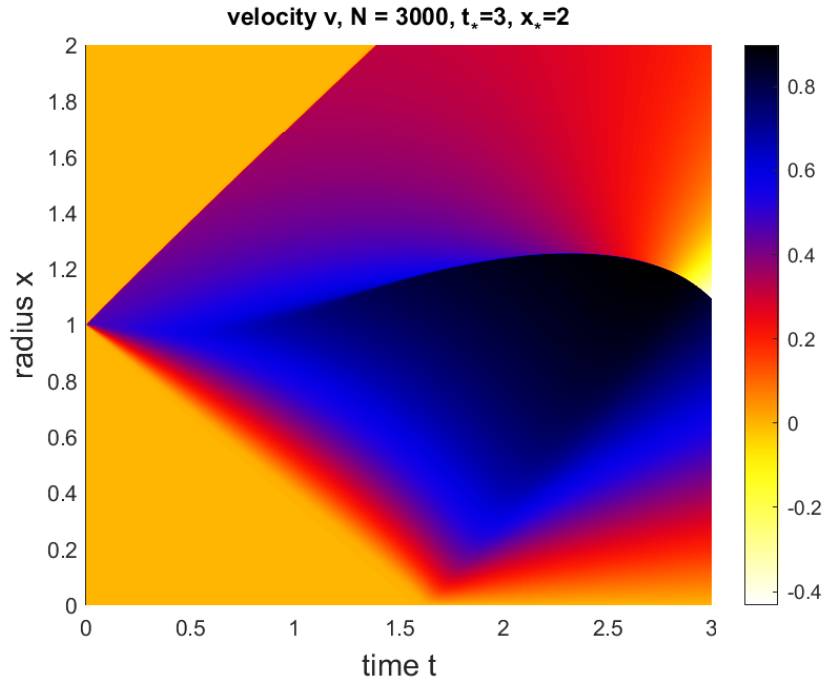
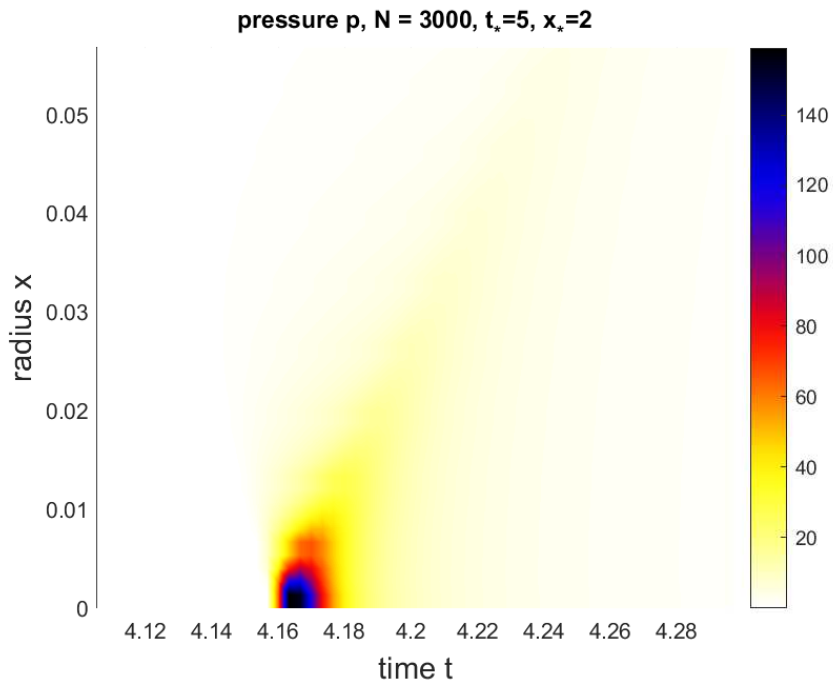
FIGURE 9. Velocity v from Example 4.

FIGURE 10. Zoom near the pressure singularity, Example 4.

For the last example we have also changed the size of the initial bubble. We only obtained the expected numerical solutions which

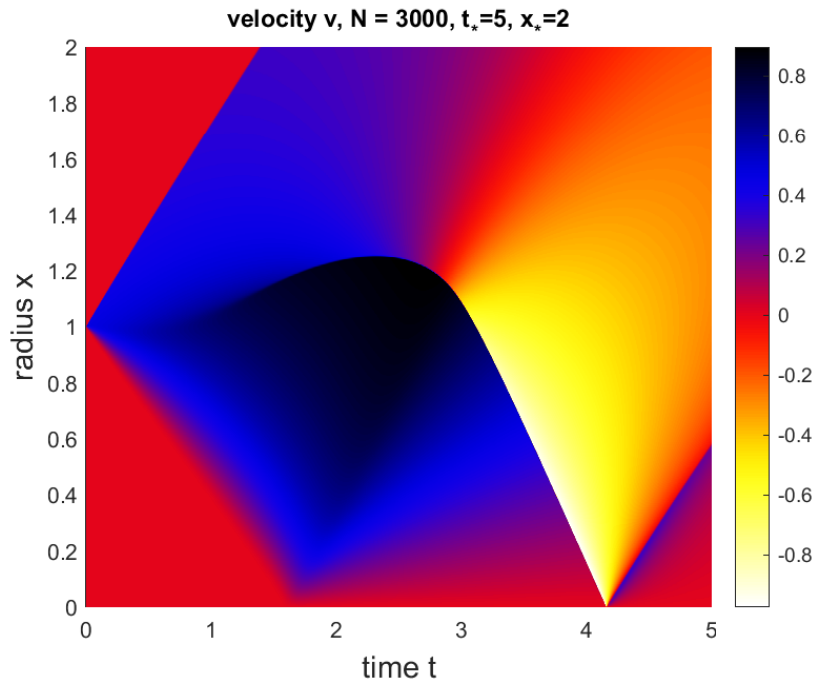


FIGURE 11. Velocity v from Example 4, extension of the solution from Figure 9 with rescaled colors .

are rescaled versions of the solutions presented here. Hence it is sufficient to study the problem with the initial bubble in the unit sphere around the origin.

Example 4 shows considerable differences in the values of the pressure, especially in the domain $(t, x) \in [4, 4.1] \times [0, 0.02]$ a pressure less than 10^{-5} . At present we restrict our study to weak solutions without a vacuum state $a = b = 0$. But a vacuum state may occur for certain initial data with symmetry and positive pressure in radially symmetric solutions of the ultra-relativistic Euler equations, see Lai's paper [14, Lemmas 2.4, 2.5; Remark 2.2]. In this case it is convenient to use the original quantities a and b for which we have developed the scheme in Section 4. The question arises whether our scheme has the capability to capture more general solutions including the vacuum state accurately.

Acknowledgement: We thank Christoph Matern and Alexander Kaina for their support in solving problems with Latex.

REFERENCES

- [1] M.A.E. Abdelrahman and M. Kunik, *The Ultra-Relativistic Euler Equations*, Math. Meth. Appl. Sci. 38, no. 7, 1247-1264, 2015.
- [2] M.A.E. Abdelrahman and M. Kunik, *The Interaction of Waves for the Ultra-Relativistic Euler Equations*, J. Math. Anal. Appl. 409, no. 2, 1140-1158, 2014.
- [3] M.A.E. Abdelrahman and M. Kunik, *A new front tracking scheme for the ultra-relativistic Euler equations*, J. Comput. Phys. 275, 213-235, 2014.
- [4] A. Bressan, *Lecture notes on hyperbolic conservation laws*, 1995.
- [5] R. Courant and K. O. Friedrichs, *Supersonic flow and shock waves*, Springer, New York, 1999.
- [6] C. M. Dafermos, *Hyperbolic Conservation Laws in Continuum Physics*, Grundlehren der mathematischen Wissenschaften, Band 325, Springer Berlin, Heidelberg, 2010.
- [7] T. Ghaffar, M. Yousaf, and S. Qamar, *Numerical solution of special ultra-relativistic Euler equations using central upwind scheme*, Results in Physics, 9:1161–1169, 2018.
- [8] W. Heineken and M. Kunik, *The analytical solution of two interesting hyperbolic problems as a test case for a finite volume method with a new grid refinement technique*, J. Comp. Appl. Math. 214(2):509–532, 2008.
- [9] H.K. Jenssen, *On radially symmetric solutions to conservation laws. Nonlinear conservation laws and applications*, IMA Vol. Math. Appl., 153, 331-351, 2011.
- [10] M. Kunik, *Selected Initial and Boundary Value Problems for Hyperbolic Systems and Kinetic Equations*, Habilitation thesis, Otto-von-Guericke University Magdeburg, 2005. The thesis is available under <https://opendata.uni-halle.de//handle/1981185920/30710>
- [11] M. Kunik, S. Qamar and G. Warnecke, *A BGK-type kinetic flux-vector splitting scheme for the ultra-relativistic Euler equations*, SIAM J. Sci. Comput. 26, no. 1, 196-223, 2004.
- [12] M. Kunik, S. Qamar and G. Warnecke, *Second order accurate kinetic schemes for the ultra-relativistic Euler equations*, Journal of Computational Physics 192, 695-726, 2003.
- [13] M. Kunik, S. Qamar and G. Warnecke, *Kinetic schemes for the ultra-relativistic Euler equations*, Journal of Computational Physics 187, 572-596, 2003.
- [14] G. Lai, *Self-similar solutions of the radially symmetric relativistic Euler equations*, European Journal of Applied Mathematics, doi:10.1017/S0956792519000317, 1-31, 2019.
- [15] S. Qamar, M. Yousaf, S. Mudasser, *The space-time CE/SE method for solving ultra-relativistic Euler equations*, Comp Phys Commun, 182:992–1004, 2011.
- [16] S. Qamar, M. Yousaf, *The space-time CESE method for solving special relativistic hydrodynamic equations*, J Comp Phys, 23:3928–3945, 2012.
- [17] S. Qamar, M. Yousaf *Application of a discontinuous Galerkin finite element method to special relativistic hydrodynamic models*, Comp Math App, 65:1220–1232, 2013.
- [18] P. He, H. Tang *An adaptive moving mesh method for two-dimensional relativistic hydrodynamics* Commun Comput Phys, 11:114–146, 2012.
- [19] O.A. Oleinik, *Discontinuous solutions of nonlinear differential equations*, Amer. Math. Soc. Trans. Ser. 26, 95–172, 1957.
- [20] H. Saran and H. Liu, *Alternating evolution (AE) schemes for hyperbolic conservation laws*, SIAM J. on Scientific Computing. 33(6), 3210–3240, 2011.
- [21] E. F. Toro, *Riemann Solvers and Numerical Methods for Fluid Dynamics: A Practical Introduction*, 2nd ed., Springer-Verlag, Berlin, 1999.
- [22] S. Weinberg, *Gravitation and Cosmology*, John Wiley, New York, 1972.

OTTO-VON-GUERICKE-UNIVERSITÄT MAGDEBURG, INSTITUT FÜR ANALYSIS UND
NUMERIK, GEBÄUDE 02, UNIVERSITÄTSPLATZ 2, D-39106 MAGDEBURG, GERMANY

E-mail address: `matthias.kunik@ovgu.de`

IOWA STATE UNIVERSITY, DEPARTMENT OF MATHEMATICS, AMES, IA 50010-
2064, USA

E-mail address: `hliu@iastate.edu`

OTTO-VON-GUERICKE-UNIVERSITÄT MAGDEBURG, INSTITUT FÜR ANALYSIS UND
NUMERIK, GEBÄUDE 02, UNIVERSITÄTSPLATZ 2, D-39106 MAGDEBURG, GERMANY

E-mail address: `gerald.warnecke@ovgu.de`